Mechanistic insights into 2,4-D photoelectrocatalytic removal from water with TiO_2 Nanotubes under dark and solar light irradiation.

Annalisa Vacca[a], Laura Mais[a]*, Michele Mascia[a], Elisabetta Maria Usai[a], Jesus Rodriguez[b] and Simonetta Palmas[a]

[a] *Dipartimento di Ingegneria Meccanica, Chimica, e dei Materiali, Università degli Studi di Cagliari, via Marengo 2, 09123 Cagliari, Italy*

[b] *Centro Nacional de Hidrógeno, Prolongación Fernando el Santo, s/n, 13500 Puertollano (Ciudad Real), Spain*

**corresponding author: laura.mais@unica.it*

Abstract

Removal of recalcitrant pollutants from water is a major challenge, to which the photoelectrocatalytic processes may be a solution. Applied potential plays a key role in the photocatalytic activity of the semiconductor. This paper investigated the effect of applied potential on the photoelectrocatalytic oxidation of 2,4-Dichlorophenoxyacetic acid (2,4-D) with TiO_2 nanotubular anodes under solar light irradiation. The process was investigated at constant potentials in different regions of the polarisation curve: the ohmic region, the saturation region and in the region of the Schottky barrier breakdown. PEC tests were performed in aqueous solutions of 2,4-D, and in the presence of methanol or formic acid, as scavengers of $OH^{\bullet}$ radicals and holes.

Results showed the main mechanism is oxidation by $OH^{\bullet}$ radicals from water oxidation, while runs with hole scavenger revealed a second mechanism of direct oxidation by holes photogenerated at the electrode surface, with high removal rates due to current doubling effect.

Keywords: photoelectrochemical degradation, TiO_2-NT structures, scavenger, current doubling effect, Schottky barrier breakdown

1. Introduction

Recalcitrant compounds such as pesticides and pharmaceuticals, are resistant to conventional chemical and biological processes [1]: very low concentration levels are required by legislation for such toxic compounds, and their removal from water remains a major challenge all over the world [2]. Among the others, 2,4-Dichlorophenoxyacetic acid (2,4-D), has been classified as the most commonly used herbicide for agricultural purpose in the last decade [3]. Due to the relevance of the possible negative effects on the environment, the degradation process of this compound has been studied for a long time and various techniques have been proposed [4][5][6][7]. A recent review [8] showed that processes such as adsorption, biological degradation, electrochemical treatments, ozonation, Fenton process, and photocatalysis, all gave good results in 2,4-D degradation. A comparison between pros and cons of the different techniques indicates adsorption as one of the best, due to its low cost, availability and ease of operation and efficiency, even if it takes higher operating time. Biological processes are considered cost effective and environmentally sustainable, but they are slow and with limited success in removing potentially toxic substances, such as

herbicides. High costs are expected for electrochemical treatment, which however may allow high removal yield, working with low-volume and high-concentration.

In order to, either limit costs or shorten treatment times, combination of techniques may be suggested, rather than a single technology, as a viable solution that synergistically contributes improving the performance of the final process [9][10][11][12]. Thus, for example, an electrochemical treatment can be coupled with a biological, in order to increase the biodegradability of the wastewater and shorten the treatment times. The costs of the process can be reduced by using photoelectrochemical (PEC) technologies, in which the energy need for the electrochemical process is compensated by the photocatalytic process.

Application of PEC processes is reported in literature in both organic synthesis [13][14] and in the removal of several organic pollutants [15]. One of the advantages of photo-assisted electrolysis is the cathodic production of H_2 which can be a process of interest along with the anodic oxidation of the pollutant [16]. Core of the PEC process is the semiconductor material where e^-/h^+ couples are originated by the incident radiation of suitable wavelength. On the other hand, the applied potential plays a key role in a PEC process, which mainly assists the transfer of photo-generated electrons towards the external circuit. It generates an increase in the potential gradient within the space charge of the semiconductor (SC), so that the recombination of the e^-/h^+ pairs may be decreased or totally prevented, thereby improving the photocatalytic performance [17]. Actually, charge recombination, along with the side reaction of holes and water to give O_2, may be the main responsible for low yield of a PEC process. The low economic value of O_2, makes this latter an unwanted reaction, especially when oxidation of the reactant is addressed to obtain compounds of higher added value [18]. In PEC systems, the applied potential may allow controlling the process also with respect to this possible side reaction.

Moreover, the applied potential may exert a strong effect on the photocatalytic activity of the semiconductor, which is mainly due to its defectivity. For example, in the case of TiO_2 different kinds of defects, such as oxygen vacancies or interstitial Ti^{+3}, may be located at different energy levels more or less far from the conduction band (CB) [19]. During the PEC process, light of a suitable wavelength causes the charge to be trapped on the defect, while the application of an oxidative potential causes its subsequent emptying. Thus, application of an increasing oxidative potential, in addition to favoring the possible O_2 evolution reaction, may lead to an increasing involvement of these defects in the oxidation reaction, and in turn, enhancing the photoactivity.

PEC activity of many SC has been tested for removal of organics: the trend of the involved reactions, as well as the performance of the process, strictly depends on the structure of the SC material, as well as on the involved pollutants and their reciprocal interactions. Typical organic pollutants such as dyes, phenol or its derivatives are generally taken as model molecules [20][21][22]: the activation of the process always originates from the formation of the e^-/h^+ pairs, but the whole path of the reaction depends on the ability of the system to exploit the charges before they recombine.

From the above, we understand the importance of studying the operating mechanism of these structures, to address their synthesis towards final electrodes with such characteristics specifically optimized with respect to the compound which has to be treated: such aspects as the photo-catalyst-dependence of a specific degradation reaction and the substrate-dependence of a given photo-catalyst are less investigated and understood so far [23].

In previous work nanotubular (NT) structures of TiO_2, obtained by oxidation of Ti sheets in the presence of fluorides, have been analysed under different operative conditions [24]; different morphologies have been synthesised, also in combination with other metal oxides and noble metals [25][26][27][28][29], to obtain electrodes that may be effective in exploiting the light at different

wavelengths, in view to broaden the application of such systems with solar light. The complex dependence between characteristics of the organic compound, such as diffusivity and reactivity, and the potential distribution has also been modelled: depending on the operative conditions, only part of the whole length of the NT was found to be active in the oxidation reaction, and in the OH radical generation [30].

Usually, investigation of PEC processes, is made in the ohmic range and in the range of saturation of the photocurrent, whereas the range where potential is higher than the SC band gap is less frequently investigated in the literature. In most of the cases at these high potentials, the physics of the diode-like behaviour of the structure was only investigated [31]. As the application is concerned, the synthesis of porous silicon structures [32][33] was studied as well as the behaviour of TiO_2 nanotubes under high potential to control wettability of the structures [34]. In these studies, pseudo photocatalytic reactions in the absence of light were observed with applied potential larger than band gap of the SC: under these conditions, the so called "Schottky barrier breakdown" occurs, where the applied voltage generates valence-band holes. Depending on doping of the semiconductor material and width of the space charge, this effect may result either in the *avalanche effect* or in the *Zener effect* [35]. In the avalanche effect, high electric field inside the space charge of the SC accelerates the charge carriers, which have enough kinetic energy to cause the generation of new electron-hole pairs. However, when the charges have not sufficient energy to break covalent bonds by impact, the electric field may enable the tunnelling of the electrons from the valence (VB) to the conduction band (CB), leading to a large number of free minority carriers which sudden increase the reverse current (Zener effect). Recent literature demonstrated that the Zener effect could be also active for undoped semiconductor materials [36].

In the present paper TiO_2 has been selected as electrode material due to its well-known characteristics of low-cost, high availability and stability [37], and a nanostructured morphology has

been prepared, so that high porosity and high defectiveness allowed increasing the response to light in a larger range of wavelength, and the challenge was to exploit this nanostructured material in the removal process of 2,4-D under solar light irradiation. Starting from the analysis of the 2,4-D removal kinetics and the efficiency of the process, we investigated the operating mechanism of the NT structure at three potential values belonging to different potential ranges of the polarization curve. The aim of the work was also understanding whether and how the different phenomena influence 2,4-D removal process in the different potential ranges. To the best of our knowledge this work presents the first study on catalysis of TiO_2 nanotubes under solar light irradiation with applied potential higher than the band gap.

2. Experimental

All the electrochemical measurements were performed with a potentiostat-galvanostat (Metrohm Autolab 302N, Metrohm Switzerland). Reagents were used as received by the producer, without any further purification. Deionised water was used to prepare aqueous solutions.

Figure 1 shows the schematic view of the electrochemical (EC) and photo-electrochemical (PEC) two-electrode cells, respectively used to prepare the TiO_2 samples, and to perform the PEC tests: they were obtained from PTFE hollow cylinders (inner diameter = 4.4 cm; height = 5 cm). In the first one (Figure 1A), with electrodes horizontally oriented, the working electrode (geometrical area of 13,5 cm^2) was located at the bottom of the cell, while a grid of platinized Ti, placed in front of the anode at 1 cm distance, constituted the counter electrode. The second one, in which the electrodes were vertically oriented, was equipped with a quartz window (PEC cell - Figure 1B) to allow the irradiation of the anode: in this case, the counter electrode was a Pt ring, located in the inner surface of the cylindrical body, in order to do not shadow the correct irradiation of the sample.

To obtain TiO_2 nanotubular structures, Ti discs (0.25 mm thickness, 99.7 % metal basis, Aldrich) were firstly submitted to three ultrasonic treatments in acetone, isopropanol and methanol (10 minutes each), then rinsed with deionized water, and dried with a nitrogen stream. Oxidation of the so-prepared Ti samples was performed in 0.14 M NH_4F water/glycerol solution (10/90 v.v). A potential ramp was imposed starting from the open circuit voltage (OCV) to a fixed potential E = 20 V with a scan rate of 100 mVs^{-1}, then maintaining this fixed potential value for 4 h. In order to transform the amorphous structure into crystalline one, a final annealing treatment was performed at 400°C for 1 h, under air atmosphere.

Photocurrent measurements were carried out by linear sweep voltammetric technique (LSV), starting from the OCV (generally measured in the range of -0.3 V to -0.2 V in dark conditions, and -0.6 V under irradiation) to 4 V at a scan rate of 10 mVs^{-1}. A 300 W xenon lamp equipped with air mass (AM) 0 and 1.5 D filters was used to simulate the solar radiation. During the runs, at regular intervals of time, the light was turned off to measure possible contribute of the dark current. Photocurrent was calculated by subtracting the stable value measured in the dark, from that obtained under irradiation.

Figure 1.

For the degradation experiments the PEC cell was inserted in a hydraulic circuit, in which the electrolyte (V = 80 cm^3) was pumped by a peristaltic pump from the reservoir throughout the cell and back in a closed loop (Figure 1 C). PEC oxidation of aqueous solutions of 2,4-Dichlorophenoxyacetic acid (2,4-D) was carried out by potentiostatic runs: a constant initial concentration of the organic compound of 50 mg dm^{-3} was used, in 0.1 M $NaClO_4$ supporting electrolyte. Depending on the runs, either methanol (MeOH) or formic acid (FA) 0.2 M were added

161 to the solution. PEC tests were performed at three different cell potential values, namely 0V, 2.5V
162 and 4V.

163 During the runs, the disappearance of the reactant, as well as the possible formation of reaction
164 intermediates were monitored by UV-Vis spectrophotometry (Agilent Technologies Cary Series
165 Spectrophotometer).

166

167 ***Figure 2.***

168

169 Spectra recorded for solutions prepared at different concentrations of 2,4-D are shown in Figure 2:
170 according to the literature [38][39] the two peaks, at 229 nm and 283 nm, were attributed to 2,4-D.
171 However, due to possible overlapping with the peak related to formic acid (also revealed at 229
172 nm), quantification of data related to 2,4-D has been made by following the trend of the peak at
173 283 nm.

174 Depending on the runs, samples were also analysed by HPLC (Waters 600-2487 dual λ) equipped
175 with a C18 column (Varian); the mobile phase was CH_3CN and 0.1% H_3PO_4 = 40:60 with a flow rate
176 of 1 mL min^{-1}. The UV-vis detector was set at 229 and 283 nm. Standard solutions of 2,4-D and some
177 typical intermediates has been also analysed. Under these analytic conditions the retention time of
178 2,4-D was 11 minutes. Comparison with standard solutions of 2,4-D, allowed quantification of the
179 related peak, and in turn to confirm the data of UV spectra within a 10% of error, possibly due to
180 the overlapping with other aromatic compounds. An example of HPLC analyses is shown in figure 3
181 for samples taken during a degradation test. As can be observed at 283 nm, the peak of 2,4-D
182 decreases and two waves appear at low retention times (4-6 minutes). Although not yet specifically
183 identified, these peaks can be attributed to aliphatic acids with low MW. At high treatment times a

184 shoulder at 12 minutes can be also observed which has been identified as 2,4-dicholorophenol
185 (2,4DCP) formed as reaction intermediate. Better resolution of the peaks related to 2,4-D and
186 2,4DCP has been obtained depending on the amount of 2,4DCP formed and on the 2,4-D residual
187 (as an example, see inset of figure 3).

188

189 ***Figure 3.***

190

191 **3. Results and Discussion**

192

193 ***Figure 4.***

194

195 Figure 4 shows an example of the final structure obtained by Ti oxidation. The tube dimensions
196 depended on the specific conditions adopted: in detail, water percentage used in the oxidation bath,
197 and duration of the potential step, were crucial in determining diameter of tubes and their length,
198 respectively [40]. Under the experimental condition adopted in the present case, a mean diameter
199 of tubes ranged between 40 – 50 nm, and a tube length of around 700 nm were measured, from
200 which a real superficial area could be estimated very higher than the geometrical one. However,
201 rather than the effective value of the surface area, the actual penetration of the electrolyte inside
202 the pores is worth to be considered. And the choice of using glycerol as organic in the anodizing
203 bath is based on this fact. Of note, in a previous work [40] the internal and external capacity of NT
204 structures obtained in water/glycerol (W/G) and water/ethylene glycol (W/EG) oxidation bath, were
205 derived by a voltammetric study: the results showed that with glycerol the micro-porosity of the

structure was limited and the electrolyte was able to exploit most of the NT structure. Instead, smaller pore diameters and a minor accessibility for the electrolyte were obtained in W/EG media, where the external area was not coincident with the total one.

Prepared samples were firstly characterized by polarization test. Figure 5

shows the linear potential sweeps in solution of 50 mg dm^{-3} 2,4-D, for electrodes irradiated with constant power light. A typical trend [41][42] is observed in the polarization curve, which may be divided in three potential regions:

Figure 5.

i) *region 1* - from the OCV value, up to about 1 V: an initial ohmic trend is observed which can be directly connected to the response of the space charge, that is originated at the surface of the nanotube walls, in the electrode/electrolyte interface. As long as the space charge extends in the wall thickness, the increase in the applied potential generates higher depletion in the space charge, which enhances the separation of the photo-generated charges, and in turn, increases the measured current.

ii) *region 2* - 1V < E < 3V: a current plateau is observed, related to the saturation range of the photocurrent. In this range, an equilibrium is reached between the rate of photo-charge generation and the rate of charge transport within the space charge layer. The electrical field established in the space charge region, separates all the photo-generated charges, so that increasing the potential does not appreciably modify the measured current.

iii) *region 3* - E > 3V: the potential is higher than the value of band gap of the SC, the photocurrent is increased by a dark current due to the barrier breakdown.

In order to study the photoelectrocatalytic process in the three potential regions, potentiostatic runs with 2,4-D solutions were carried out at three cell potentials equal to 0 V, 2.5 V and 4 V, being the other operative conditions (irradiation and electrolyte flow rate) the same.

Quantification of the UV spectra of samples withdrawn during electrolyses performed at the different cell potentials, allowed deriving data in Figure 6: indication on the kinetics can be deduced from figure 6 a) where the logarithm of 2,4-D concentration, normalized with the initial value, is reported as a function of time, while the trend of fraction of the removed reactant as a function of the specific supplied charge (Figure 6b) gives indication on the yield of the process. Data indicate that while the highest reaction rate is achieved for runs at 2.5V, (region 2 of figure 5), the highest yield of the removal process is measured at the lowest potential, in region 1: in this region most of the current causes the removal of the reactant (70% removal is measured after 150 C dm^{-3}), while at 2.5 V (*region 2),* and especially at 4 V (region *3),* the reagent removal efficiency is significantly lower (60% removal, and 20% after about 300 C dm^{-3}, respectively), and wide part of the charge is dedicated to other reactions, namely O_2 evolution from oxidation of the solvent.

Figure 6.

Additional electrolysis was carried out at 4 V under dark conditions and no appreciable decrease in the peak of the main reactant was revealed.

In the next phase of the work, attention was paid to investigate whether, in addition to a different performance, operating at different potentials also led to a different reaction mechanism. To this aim, data on the reagent oxidation were analyzed in the presence of a scavenger.

Generally, scavengers are used to improve the process of interest: a hole scavenger is adopted to make free the electrons and speed the reduction process up, while an electron scavenger is adopted to release the holes and increase the rate of the anodic process. In our case, to investigate on the oxidative reaction mechanism of 2,4-D, we used two kinds of scavengers, which were both expected to affect the anodic process: i) methanol (MeOH), which is a typical scavenger of $OH^{\bullet}$ radicals originated from the oxidation of water by the holes; ii) formic acid (FA) which is a typical hole scavenger.

The results, as semi-logarithmic trend of normalized concentration of 2,4-D are reported in figure 7. Data indicated that a different effect was exerted by the two scavengers, depending on the applied potential. In *region 1* both scavengers determined a negative effect on the process: lower removal yield was measured, when either MeOH or FA were present in solution. In this potential range, the electron transport within the TiO_2 film is the rate-limiting step and the system behaves like a pure resistor [41]; the increase in applied potential enhances the separation of the photo-generated charges, making a higher h^+ concentration available to react with the donor. The effectiveness of the organic removal process depends on the reactivity of the compound towards $OH^{\bullet}$ radicals or holes: any side process that subtracts either $OH^{\bullet}$ radicals decreases the yield of the main process.

The two scavengers had different effects when runs were performed at 2.5 V and 4 V: in *regions 2* and *3* the negative effect of MeOH still resulted in a lower 2,4-D removal yield, while FA exerted a positive effect, resulting in a slight increased yield in *region 2*, which became more evident in *region 3*.

Figure 7.

The kinetics of the 2,4-D removal was also analyzed: the trend with time of 2,4-D concentration is linear in a semi-logarithmic plot, both in solutions with only 2,4-D and in the presence of scavengers (data not reported). The pseudo-first order kinetic constants, evaluated by linear regression of data, are shown in Figure 8.

Figure 8.

As can be observed, regardless the presence of scavengers, the main reaction is faster in *region 2*; moreover, MeOH always has a negative effect and it tends to slow reaction rate down. Different effect of FA is revealed also from these data: as for yield data, it has a positive effect in *regions 2* and *3*; while in *region 1*, where a negative effect on the yield was recorded, an almost negligible effect on the kinetics is also measured.

To complete the analysis of the PEC processes under the different conditions, also the values of current measured at the different potentials are compared (Figure 9): of note, even if the reactant concentration decreased with time, a nearly constant value of current was recorded after the initial few seconds, due to water electrolysis. During the runs, dark currents were also measured, turning the light off: this allowed verifying the absence of current dark contribute in *regions 1* and *2*; the dark currents for runs in *region 3* are reported in figure 9. Of note, the dark current contribute is almost constant, regardless the presence of scavenger. An increase in photocurrent is instead measured especially when FA is added to the solution.

Figure 9.

Considering the total current measured during PEC runs, except in region 1, where the MeOH effect seems to be almost negligible, the addition of the two scavengers always generates an increase in the total current, compared to that measured when only 2,4-D is in solution; however, the increase measured in the presence of FA is significantly higher.

On the basis of the presented results the removal of 2,4-D at NT TiO_2 may be described by two mechanisms: the first one, which appears to predominate in most cases, occurs by $OH^{\bullet}$ radicals generated by water oxidation, while the second one may also be active in parallel, through direct oxidation of 2,4-D by the photo-generated holes. Previous work, indicated that a different distribution of reaction products should be expected depending on the prevailing mechanism [43]: if the process took place by direct oxidation by the holes, the reaction was mainly localized on the -COOH group linked to the aromatic ring, and the products were 2,4-dichlorophenol, 2,4-dichlorophenol formate, formaldehyde and CO_2. When the process occurred by OH radical, the yield in these products was low, indicating that in this case the aromatic ring was directly involved in the reaction.

In the present work the competitive effect exerted by MeOH has been already highlighted as indication of a reaction contribution mediated by $OH^{\bullet}$ radicals. HPLC analysis of samples withdrawn during the runs, confirmed this mechanism in most of PEC experiments. Figure 10 shows the comparison between chromatograms obtained for samples treated at 0 V, 2.5 V and 4 V under solar light irradiation, the supplied electric charge being the same. In the three regions the decrease of the 2,4-D peak, due to the opening of the aromatic ring, and the related appearance of aliphatic intermediates can be observed. Different trend is observed at 4V under dark conditions, where a

direct oxidation by the holes may occur. As can be seen (see black line in figure 10) the initial peak at 11 minutes does not change during the electrolysis, even if aliphatic intermediates are formed: this behaviour can be explained considering the conversion of 2,4-D in aliphatic acids and 2,4DCP which overlaps with the signal of 2,4-D.

Figure 10.

To correctly describe the working mechanism of the structure and to understand the prevailing oxidative pathway under the different operative conditions, several factors need to be considered, mainly connected to both the electrochemical and photo-chemical response of the system.

From the photo-chemical point of view, it must be considered that we are in the presence of a heterogeneous PEC process, in which TiO_2 is working as a photo-anode. The light with energy greater than the band gap, which arrives on its active sites, is able to generate electrons and holes: they must diffuse towards the external circuit, the former, and towards the interphase surface, the latter. Then, holes may be trapped on the surface sites where they will meet the surface-adsorbed reducing agents, thus activating the direct oxidation reactions of the organic contained in the electrolyte. Bulk recombination represents the main competitor to this process. Since recombination is an ultrafast process, to allow the slower chemistry to effectively compete with recombination, donors need to be pre-adsorbed at the photo-anode surface sites [44].

In aqueous solution, hydroxyl ions OH^- or water molecules must be considered among the possible competitors, for photo-generated holes [45]. An additional donor, such as a hole scavenger, may also compete with the organic, both in terms of oxidation, i.e. possibility of exploiting the photo-

generated holes, and of adsorption: a strongly bounded scavenger can decrease or even totally prevent the adsorption of the organic.

Preliminary indications on the reactivity of the two scavengers have been derived from potentiostatic tests, carried out with solutions only containing the scavengers (Figure 11).

Figure 11.

During the tests with MeOH in the ohmic range, a high current spike is measured which drops rapidly due to recombination: MeOH reacts mainly with $OH^{\bullet}$ radicals, so that it is not able to directly interfere with the e^-/h^+ recombination process.

Higher current values are recorded in the presence of FA in the three regions, and a flat step of the current is measured even at low potential: FA mainly reacts by direct oxidation with holes, keeping them separated from the e^- thus avoiding recombination. At the highest potentials, in *region 3*, an increasing trend of the recorded current with FA is observed, which may be attributed to the so-called "current doubling effect" [46]. Such a phenomenon is generally observed when an organic or inorganic sacrificial agent is added to the electrolyte in a PEC cell. The effect was firstly observed, in the presence of HCOONa, during the water photo-electrolysis on ZnO [47]: in the presence of HCOONa, the photo-generated holes interact with $HCOO^-$ ions producing intermediate radical species.

$$HCOO^- + h^+ \rightarrow HCOO^{\bullet}$$

Such radical is unstable, and it decomposes liberating a hydrogen ion and an electron which is injected into the conduction band of the semiconductor:

363 $HCOO^{\bullet} \rightarrow CO_2 + H^+ + e^-$

364 Therefore, for one photon absorbed, one electron is photo-generated and one is injected by the
365 radical, i.e. two electrons are produced for one photon absorbed, so that the final current is
366 doubled.

367 The above effect could be responsible for the higher currents recorded in the three *region*s, related
368 to FA, compared to those related to MeOH.

369 In this framework, the effect of the two scavengers may be described as follows:

370 *MeOH* - while not causing an increase in current, it subtracts $OH^{\bullet}$ radicals, and therefore, electrical
371 current being the same, the final effect is a decrease in both the kinetics and the reactant removal
372 efficiency.

373 *FA* - the addition of FA raises the current, since both the doubling effect and the capture of holes
374 release a greater amount of e^- towards the external circuit; however, the presence of FA reduces
375 the removal efficiency because part of the total current is used for its oxidation.

376 The fact that in *region 1* the reactant removal rate is not modified by the presence of FA, indicates
377 the reactions of 2,4-D removal and FA oxidation are independent: two different sites could be
378 involved in the two reactions. In a previous work on oxidation of FA with Degussa P25, two kinds of
379 sites were mainly involved with different adsorption strength [48]. In particular, oxygen vacancies,
380 identifiable as Ti^{+3}, which normally accounts for about 10-12% of the defectivity [49], are likely to
381 accommodate the dissociated form of the molecules (i.e. FA^-), while the undissociated form was
382 more weakly linked on Ti^{+4} sites [48]. Other authors determined that FA adsorbs on two adsorption
383 sites in TiO_2: the first site (25% of the total) is selective towards formate ions, the second towards
384 undissociated acid. The two forms of adsorbed formate react with significantly different rates
385 [50][51].

386 The different nature of active sites could partially justify the trend of the removal data recorded in
387 *regions 2* and *3*. Moreover, the effect of pH could be also considered because it may influence both
388 the superficial charge of the electrode (pzc = 6) and the dissociation equilibrium of reactant (pKa of
389 2,4-D =2.9 [43]) and scavenger (pKa of FA = 3.77 [52]), and in turn the reaction mechanism. pH values
390 of the 2,4-D solutions were always in the range of 3.8 – 4, and they did not change appreciably in
391 the presence of MeOH. The highest pH variation was measured in the presence of FA, with a value
392 of 2.6. Under these conditions, a decrease in adsorption could occur, due to the weaker interaction
393 between the undissociated FA molecule and the TiO_2 surface, positively charged [23]: the
394 consequent lower reactivity of the scavenger makes it less interfering with the main reaction. Such
395 effects can justify the result obtained in *region 1*, in which the kinetics of the 2,4-D removal is not
396 modified by the presence of the FA. However, it cannot justify the result obtained in *regions 2* and
397 *3*, in which the presence of FA accelerates the 2,4-D removal. This suggests that other factors are
398 influencing the electrode activity: since we are dealing with a PEC process, the effect of the applied
399 potential cannot be neglected.

400 As pointed out in our previous work [30], the applied potential may determine the fraction of NT
401 surface which remains active in the oxidation reaction, and in the OH radical generation; moreover,
402 it determines the involvement of the different kinds of defects, located at different energy levels in
403 the band gap. Thus, depending on the distribution of surface and bulk defects, and on the potential
404 gradient within the structure, the quasi-Fermi level could be pinned at the surface and, at the same
405 time, it can be strongly shifted to higher potentials, in the bulk of the structure, so that in some
406 points it could reach or exceed the energy level of the valence band (VB). Thus, as mentioned in
407 Introduction, when the applied potential is higher than the band gap of the SC, the *Schottky barrier*
408 *breakdown* may occur which could activate pseudo photocatalytic reactions by valence-band holes
409 generation [34]. Under the operative conditions of this work, the width of the space charge is

410 constrained in the NT walls and the Zener effect is likely responsible for the high dark current in this
411 range [53]. The additional run, performed in the dark conditions at 4V, shows that most of the holes
412 originated at this high potential react with water to give oxygen via OH radicals so that low reactant
413 removal is measured. As pointed out above, this low reactant removal seems to proceed via direct
414 hole reaction involving the carboxyl group of the molecule, rather than the aromatic ring, being
415 2,4DCP found in the intermediate products of the reaction [38]. The low reactant removal may be
416 attributed to the low conductivity of the structure in dark condition, which leads to potential
417 distribution within the NT. Under these conditions, the highest values of potential, and the
418 consequent breakdown of the barrier could be only reached on the final part of the NT, in direct
419 contact with the Ti substrate where the transfer of electrons can be easier. The external part of the
420 NT in direct contact with the bulk electrolyte, could not be active. Thus, reaction rate may be limited
421 by diffusion of the reactant within the pores, with the reactive part of tubes only partially reached
422 by the organics.

423 When light is on, the photo-response of NTs is activated, its conductivity increased and also their
424 outermost part could take part to the process.

425 The positive effect of FA on 2,4-D removal process may be due to the synergistic effect of the light,
426 which starts the current doubling effect, and of the applied potential, which activates deep
427 energetic levels far from the conduction band of the SC.

428

429 ## 4. Conclusions

430 The present work tested the performance of simple NT TiO_2 structure as anodes for photo-
431 electrolysis of 2,4-Dichlorophenoxyacetic acid (2,4-D) under solar light irradiation. The work allowed
432 to clarify the complex working mechanism of the electrode, under the different operative

433 conditions: several factors has been considered connected other than to the nature of the organic
434 to be removed, also to the morphology of the structure, to its semiconductor behaviour, and to its
435 response to the contemporary action of light and applied potential.
436 The results demonstrated that the synthesized NT TiO_2 structure is able to remove 2,4-D by two
437 different parallel mechanisms, which can be activated at different sites of the structure. The most
438 important one occurs trough $OH^{\bullet}$ radicals originated by the water oxidation: in fact, the yield of the
439 reactant removal is always lowered by the presence of MeOH, which is a typical $OH^{\bullet}$ radical
440 scavenger. The reaction proceeds via aromatic ring attack, and the most probable products are
441 aliphatic ones. A second mechanism, by direct oxidation due to the holes photogenerated at the
442 electrode surface, has been revealed by using FA as hole scavenger: its extent depends on the
443 conditions. When runs are performed in *region 1*, FA causes a decrease in the removal yield, while
444 the kinetics of the process is almost the same as in absence of scavenger; positive effect of FA starts
445 becoming evident for runs in *region 2* in terms of removal yield and especially of kinetics. The
446 greatest differences between runs with- and without- FA are measured in *region* 3, both in terms of
447 yield and kinetic constants. Particular attention has been paid to analyse the behaviour of the
448 structure in the highest ranges of potential.
449 In addition to assisting the transfer of photogenerated electrons towards the external circuit, the
450 applied potential contributes to increase the electric field inside the charge space of the SC, which
451 in turn may determine a different reactivity of the NT surface, also involving energetic levels deeply
452 located in the band gap. The dark current connected to the possible barrier breakdown effect,
453 resulted less active for the removal of the reactant, which occurs by direct attack of holes to the
454 carboxylic group, rather than by the aromatic ring opening. Thus, the effect of current doubling
455 activated by the FA can be assumed as responsible for the increase in the reaction rate of removal
456 of the reactant recorded in *region 2* and especially in *region 3*.

Acknowledgements

This paper is part of the research project funded by P.O.R. SARDEGNA F.S.E. 2014-2020 - Axis III Education and Training, Thematic Goal 10, Specific goal 10.5, Action partnership agreement 10.5.12 - "Call for funding of research projects - Year 2017". Authors also acknowledge the financial support of Fondazione di Sardegna, Projects CUP F71I17000280002-2017 and CUP F71I17000170002.

464 *References*

465

466 [1] T.A. Kurniawan, W.H. Lo, G.Y.S. Chan, Physico-chemical treatments for removal of
467 recalcitrant contaminants from landfill leachate, J. Hazard. Mater. 129 (2006) 80–100.
468 https://doi.org/10.1016/j.jhazmat.2005.08.010.

469 [2] D. Seibert, C.F. Zorzo, F.H. Borba, R.M. de Souza, H.B. Quesada, R. Bergamasco, A.T.
470 Baptista, J.J. Inticher, D. Seibert, C.F. Zorzo, F.H. Borba, R.M. de Souza, H.B. Quesada, R.
471 Bergamasco, A.T. Baptista, J.J. Inticher, Occurrence, statutory guideline values and removal
472 of contaminants of emerging concern by Electrochemical Advanced Oxidation Processes: A ,
473 Sci. Total Environ. 748 (2020) 141527. https://doi.org/10.1016/j.scitotenv.2020.141527.

474 [3] E. Celis, P. Elefsiniotis, N. Singhal, Biodegradation of agricultural herbicides in sequencing
475 batch reactors under aerobic or anaerobic conditions, Water Res. (2008).
476 https://doi.org/10.1016/j.watres.2008.04.008.

477 [4] Evy Alice Abigail M, Melvin Samuel S, S. Needhidasan, C. Ramalingam, Stratagems employed
478 for 2,4-dichlorophenoxyacetic acid removal from polluted water sources, Clean Technol.
479 Environ. Policy. (2017). https://doi.org/10.1007/s10098-017-1371-8.

480 [5] M.P. Serbent, A.M. Rebelo, A. Pinheiro, A. Giongo, L.B.B. Tavares, Biological agents for 2,4-
481 dichlorophenoxyacetic acid herbicide degradation, Appl. Microbiol. Biotechnol. (2019).
482 https://doi.org/10.1007/s00253-019-09838-4.

483 [6] P. Muszyński, M.S. Brodowska, T. Paszko, Occurrence and transformation of phenoxy acids
484 in aquatic environment and photochemical methods of their removal: a review, Environ. Sci.
485 Pollut. Res. (2020). https://doi.org/10.1007/s11356-019-06510-2.

486 [7] J.O. Ighalo, A.G. Adeniyi, A.A. Adelodun, Recent advances on the adsorption of herbicides

and pesticides from polluted waters: Performance evaluation via physical attributes, J. Ind. Eng. Chem. (2020). https://doi.org/10.1016/j.jiec.2020.10.011.

[8] N.S. Trivedi, S.A. Mandavgane, Fundamentals of 2, 4 Dichlorophenoxyacetic Acid Removal from Aqueous Solutions, Sep. Purif. Rev. (2018). https://doi.org/10.1080/15422119.2018.1450765.

[9] C. Zhang, Y. Li, H. Shen, D. Shuai, Simultaneous coupling of photocatalytic and biological processes: A promising synergistic alternative for enhancing decontamination of recalcitrant compounds in water, Chem. Eng. J. 403 (2021) 80–100. https://doi.org/10.1016/j.cej.2020.126365.

[10] N. Mameda, H. Park, K.H. Choo, Hybrid electrochemical microfiltration treatment of reverse osmosis concentrate: A mechanistic study on the effects of electrode materials, Desalination. 493 (2020). https://doi.org/10.1016/j.desal.2020.114617.

[11] S. Anandan, V. Kumar Ponnusamy, M. Ashokkumar, A review on hybrid techniques for the degradation of organic pollutants in aqueous environment, Ultrason. Sonochem. 67 (2020) 105130. https://doi.org/10.1016/j.ultsonch.2020.105130.

[12] A. Fellah Jahromi, M. Elektorowicz, Modified electrochemical processes for industrial-scale treatment of wastewater having high TKN content, Electrochim. Acta. 354 (2020) 136724. https://doi.org/10.1016/j.electacta.2020.136724.

[13] M.D. Kärkäs, Electrochemical strategies for C-H functionalization and C-N bond formation, Chem. Soc. Rev. 47 (2018) 5786–5865. https://doi.org/10.1039/c7cs00619e.

[14] C. Wan, R.J. Song, J.H. Li, Electrooxidative 1,2-Bromoesterification of Alkenes with Acids and N-Bromosuccinimide, Org. Lett. 21 (2019) 2800–2803.

https://doi.org/10.1021/acs.orglett.9b00771.

[15] A.M. Polcaro, A. Vacca, S. Palmas, M. Mascia, Electrochemical treatment of wastewater containing phenolic compounds: Oxidation at boron-doped diamond electrodes, J. Appl. Electrochem. 33 (2003) 885–892. https://doi.org/10.1023/A:1025815828503.

[16] S. Palmas, A.M. Polcaro, J.R. Ruiz, A. Da Pozzo, M. Mascia, A. Vacca, TiO2 photoanodes for electrically enhanced water splitting, Int. J. Hydrogen Energy. 35 (2010) 6561–6570. https://doi.org/10.1016/j.ijhydene.2010.04.039.

[17] Y.P. Peng, E. Yassitepe, Y.T. Yeh, I. Ruzybayev, S.I. Shah, C.P. Huang, Photoelectrochemical degradation of azo dye over pulsed laser deposited nitrogen-doped TiO 2 thin film, Appl. Catal. B Environ. 125 (2012) 465–472. https://doi.org/10.1016/j.apcatb.2012.06.004.

[18] T. Li, T. Kasahara, J. He, K.E. Dettelbach, G.M. Sammis, C.P. Berlinguette, Photoelectrochemical oxidation of organic substrates in organic media, Nat. Commun. 8 (2017) 6–10. https://doi.org/10.1038/s41467-017-00420-y.

[19] X. Pan, M.Q. Yang, X. Fu, N. Zhang, Y.J. Xu, Defective TiO2 with oxygen vacancies: Synthesis, properties and photocatalytic applications, Nanoscale. 5 (2013) 3601–3614. https://doi.org/10.1039/c3nr00476g.

[20] A. Vacca, L. Mais, M. Mascia, E.M. Usai, S. Palmas, Design of experiment for the optimization of pesticide removal from wastewater by photo-electrochemical oxidation with tio2 nanotubes, Catalysts. 10 (2020). https://doi.org/10.3390/catal10050512.

[21] L. Mais, M. Mascia, S. Palmas, A. Vacca, Photoelectrochemical oxidation of phenol with nanostructured TiO2-PANI electrodes under solar light irradiation, Sep. Purif. Technol. 208 (2019) 153–159. https://doi.org/10.1016/j.seppur.2018.03.074.

[22] L. Mais, A. Vacca, M. Mascia, E.M. Usai, S. Tronci, S. Palmas, Experimental study on the optimisation of azo-dyes removal by photo-electrochemical oxidation with TiO2 nanotubes, Chemosphere. 248 (2020) 125938. https://doi.org/10.1016/j.chemosphere.2020.125938.

[23] J. Zhong, Y. Zhao, L. Ding, H. Ji, W. Ma, C. Chen, J. Zhao, Opposite photocatalytic oxidation behaviors of BiOCl and TiO2: Direct hole transfer vs. indirect [rad]OH oxidation, Appl. Catal. B Environ. 241 (2019) 514–520. https://doi.org/10.1016/j.apcatb.2018.09.058.

[24] S. Palmas, A. Da Pozzo, M. Mascia, A. Vacca, A. Ardu, R. Matarrese, I. Nova, Effect of the preparation conditions on the performance of TiO2 nanotube arrays obtained by electrochemical oxidation, Int. J. Hydrogen Energy. 36 (2011) 8894–8901. https://doi.org/10.1016/j.ijhydene.2011.04.105.

[25] R. Matarrese, M. Mascia, A. Vacca, L. Mais, E. Usai, M. Ghidelli, L. Mascaretti, B. Bricchi, V. Russo, C. Casari, A. Libassi, I. Nova, S. Palmas, Integrated Au/TiO <inf>2</inf> nanostructured photoanodes for photoelectrochemical organics degradation, Catalysts. 9 (2019). https://doi.org/10.3390/catal9040340.

[26] S. Palmas, P.A. Castresana, L. Mais, A. Vacca, M. Mascia, P.C. Ricci, TiO<inf>2</inf>-WO<inf>3</inf> nanostructured systems for photoelectrochemical applications, RSC Adv. 6 (2016). https://doi.org/10.1039/c6ra18649a.

[27] Q. Wang, H. Li, X. Yu, Y. Jia, Y. Chang, S. Gao, Morphology regulated Bi2WO6 nanoparticles on TiO2 nanotubes by solvothermal Sb3+ doping as effective photocatalysts for wastewater treatment, Electrochim. Acta. (2020). https://doi.org/10.1016/j.electacta.2019.135167.

[28] Z. Liu, Y. Song, Q. Wang, Y. Jia, X. Tan, X. Du, S. Gao, Solvothermal fabrication and construction of highly photoelectrocatalytic TiO2 NTs/Bi2MoO6 heterojunction based on titanium mesh, J. Colloid Interface Sci. 556 (2019) 92–101.

554 https://doi.org/10.1016/j.jcis.2019.08.038.

555 [29] Z. Liu, Q. Wang, X. Tan, S. Zheng, H. Zhang, Y. Wang, S. Gao, Solvothermal preparation of
556 Bi/Bi2O3 nanoparticles on TiO2 NTs for the enhanced photoelectrocatalytic degradation of
557 pollutants, J. Alloys Compd. 815 (2020) 152478.
558 https://doi.org/10.1016/j.jallcom.2019.152478.

559 [30] L. Mais, M. Mascia, S. Palmas, A. Vacca, Modelling of photo-electrocatalytic behaviour of
560 TiO<inf>2</inf> nanotubes under solar light irradiation, Chem. Eng. J. 383 (2020).
561 https://doi.org/10.1016/j.cej.2019.123136.

562 [31] S.M. Sze, K.K. Ng, Physics of Semiconductor Devices, 2006.
563 https://doi.org/10.1002/0470068329.

564 [32] P. Schmuki, L.E. Erickson, D.J. Lockwood, Light emitting micropatterns of porous si created
565 at surface defects, Phys. Rev. Lett. 80 (1998) 4060–4063.
566 https://doi.org/10.1103/PhysRevLett.80.4060.

567 [33] P. Schmuki, L.E. Erickson, Selective high-resolution electrodeposition on semiconductor
568 defect patterns, Phys. Rev. Lett. 85 (2000) 2985–2988.
569 https://doi.org/10.1103/PhysRevLett.85.2985.

570 [34] Y.Y. Song, P. Roy, I. Paramasivam, P. Schmuki, Voltage-induced payload release and
571 wettability control on TiO2 and TiO2 nanotubes, Angew. Chemie - Int. Ed. 49 (2010) 351–
572 354. https://doi.org/10.1002/anie.200905111.

573 [35] D. Aulianida, S.I. Liestyasari, S.R. Ch, Semiconductor Devices, in: J. Chem. Inf. Model., 2019:
574 pp. 1689–1699.

575 [36] Y. Gupta, P. Arun, Zener behaviour of p-SnS/ZnO and p-SnS/ZnS heterojunctions, Mater.

576 Res. Express. 5 (2018). https://doi.org/10.1088/2053-1591/aab400.

577 [37] K. Nakata, A. Fujishima, TiO 2 photocatalysis: Design and applications, J. Photochem.
578 Photobiol. C Photochem. Rev. 13 (2012) 169–189.
579 https://doi.org/10.1016/j.jphotochemrev.2012.06.001.

580 [38] Y. Tang, S. Luo, Y. Teng, C. Liu, X. Xu, X. Zhang, L. Chen, Efficient removal of herbicide 2,4-
581 dichlorophenoxyacetic acid from water using Ag/reduced graphene oxide co-decorated
582 TiO2 nanotube arrays, J. Hazard. Mater. 241–242 (2012) 323–330.
583 https://doi.org/10.1016/j.jhazmat.2012.09.050.

584 [39] V. Rodríguez-González, A. Moreno-Rodríguez, M. May, F. Tzompantzi, R. Gómez, Slurry
585 photodegradation of 2,4-dichlorophenoxyacetic acid: A comparative study of impregnated
586 and sol-gel In2O3-TiO2 mixed oxide catalysts, J. Photochem. Photobiol. A Chem. 193 (2008)
587 266–270. https://doi.org/10.1016/j.jphotochem.2007.07.005.

588 [40] S. Palmas, A. Da Pozzo, F. Delogu, M. Mascia, A. Vacca, G. Guisbiers, Characterization of TiO
589 2 nanotubes obtained by electrochemical anodization in organic electrolytes, J. Power
590 Sources. (2012). https://doi.org/10.1016/j.jpowsour.2012.01.007.

591 [41] D. Jiang, H. Zhao, S. Zhang, R. John, Characterization of Photoelectrocatalytic Processes at
592 Nanoporous TiO 2 Film Electrodes: Photocatalytic Oxidation of Glucose, J. Phys. Chem. B.
593 107 (2003) 12774–12780. https://doi.org/10.1021/jp0307349.

594 [42] S. Palmas, A. Da Pozzo, M. Mascia, A. Vacca, R. Matarrese, I. Nova, Photo-electrochemical
595 behavior at different wavelengths of electrochemically obtained TiO 2 nanotubes, J. Appl.
596 Electrochem. (2012). https://doi.org/10.1007/s10800-012-0456-7.

597 [43] Y. Sun, J.J. Pignatello, Evidence for a Surface Dual Hole-Radical Mechanism in the TiO2

598 Photocatalytic Oxidation of 2,4-Dichlorophenoxyacetic Acid, Environ. Sci. Technol. 29 (1995)
599 2065–2072. https://doi.org/10.1021/es00008a028.

600 [44] N. Serpone, D. Lawless, R. Khairutdinov, E. Pelizzetti, Subnanosecond relaxation dynamics in
601 TiO2 colloidal sols (particle sizes Rp = 1.0-13.4 nm). Relevance to heterogeneous
602 photocatalysis, J. Phys. Chem. (1995). https://doi.org/10.1021/j100045a027.

603 [45] N. Serpone, I. Texier, A. V. Emeline, P. Pichat, H. Hidaka, J. Zhao, Post-irradiation effect and
604 reductive dechlorination of chlorophenols at oxygen-free TiO2/water interfaces in the
605 presence of prominent hole scavengers, J. Photochem. Photobiol. A Chem. (2000).
606 https://doi.org/10.1016/S1010-6030(00)00348-8.

607 [46] P. Herrasti, L. Peter, Photocurrent doubling during the oxidation of formic acid at n-CdS: an
608 investigation by intensity modulated photocurrent spectroscopy, J. Electroanal. Chem.
609 (1991). https://doi.org/10.1016/0022-0728(91)85522-Q.

610 [47] S.R. Morrison, T. Freund, Chemical role of holes and electrons in ZnO photocatalysis, J.
611 Chem. Phys. 47 (1967) 1543–1551. https://doi.org/10.1063/1.1712115.

612 [48] D.S. Muggli, M.J. Backes, Two active sites for photocatalytic oxidation of formic acid on
613 TiO2: Effects of H2O and temperature, J. Catal. 209 (2002) 105–113.
614 https://doi.org/10.1006/jcat.2002.3640.

615 [49] S. Wendt, R. Schaub, J. Matthiesen, E.K. Vestergaard, E. Wahlström, M.D. Rasmussen, P.
616 Thostrup, L.M. Molina, E. Lægsgaard, I. Stensgaard, B. Hammer, F. Besenbacher, Oxygen
617 vacancies on TiO2(1 1 0) and their interaction with H2O and O2: A combined high-resolution
618 STM and DFT study, Surf. Sci. 598 (2005) 226–245.
619 https://doi.org/10.1016/j.susc.2005.08.041.

[50] G.Y. Popova, T. V. Andrushkevich, Y.A. Chesalov, E.S. Stoyanov, In situ FTIR study of the adsorption of formaldehyde, formic acid, and methyl formiate at the surface of TiO2 (anatase), Kinet. Catal. (2000). https://doi.org/10.1023/A:1026681321584.

[51] L.F. Liao, W.C. Wu, C.Y. Chen, J.L. Lin, Photooxidation of formic acid vs formate and ethanol vs ethoxy on TiO2 and effect of adsorbed water on the rates of formate and formic acid photooxidation, J. Phys. Chem. B. 105 (2001) 7678–7685. https://doi.org/10.1021/jp003541j.

[52] M.S. Bradley, Chemistry, Fifth Edition (Chang, Raymond), J. Chem. Educ. 71 (1994) A289. https://doi.org/10.1021/ed071pa289.1.

[53] B.A. Briones, Wiley Encyclopedia of Electrical and Electronics Engineering, Charlest. Advis. (2019). https://doi.org/10.5260/chara.21.2.51.

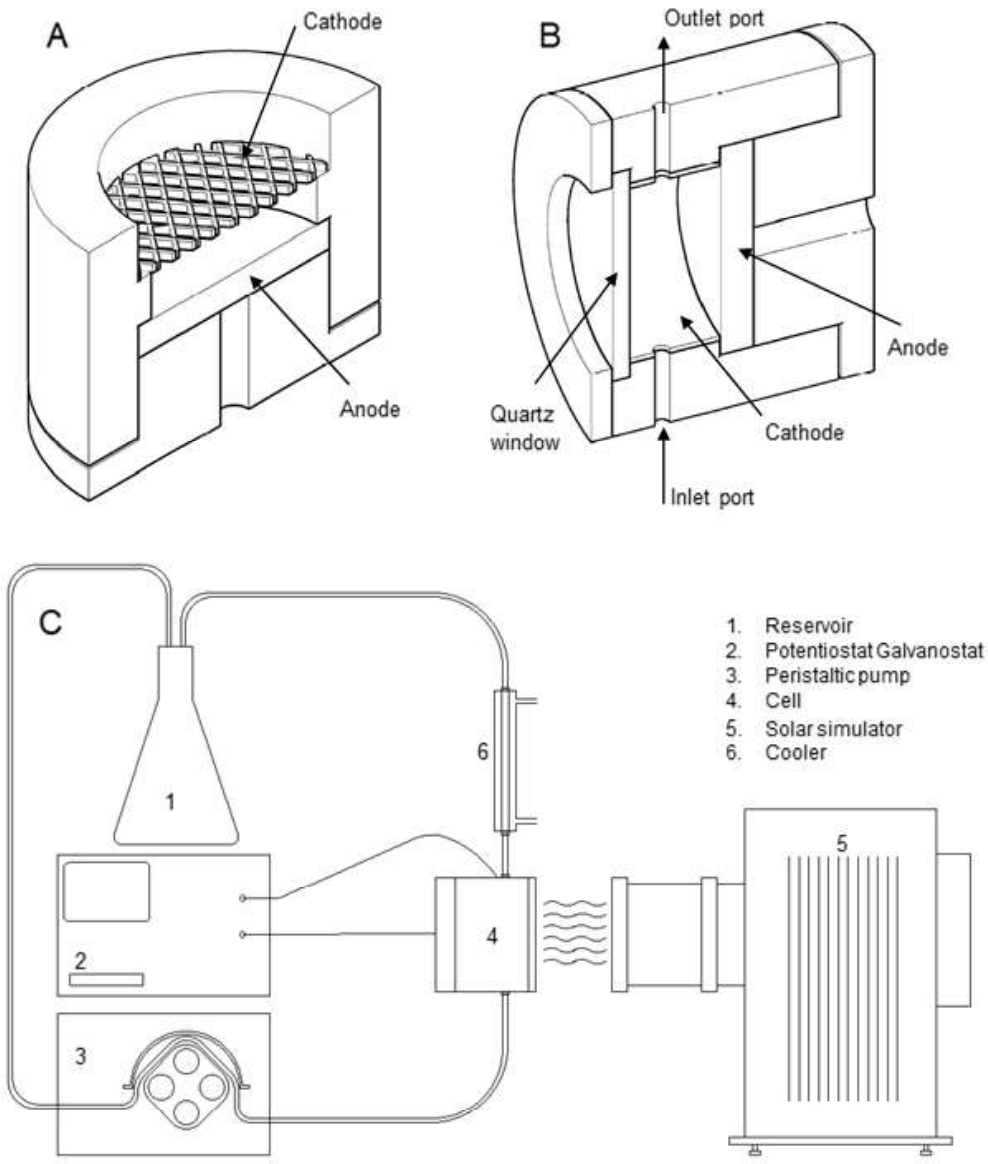

633

634 ***Figure 1.*** *Axonometric sections of the cells used in Ti foil anodization (EC cell -A) and photo-*

635 *electrochemical tests (PEC cell – B); sketch of the apparatus used for PEC experiments (C).*

636

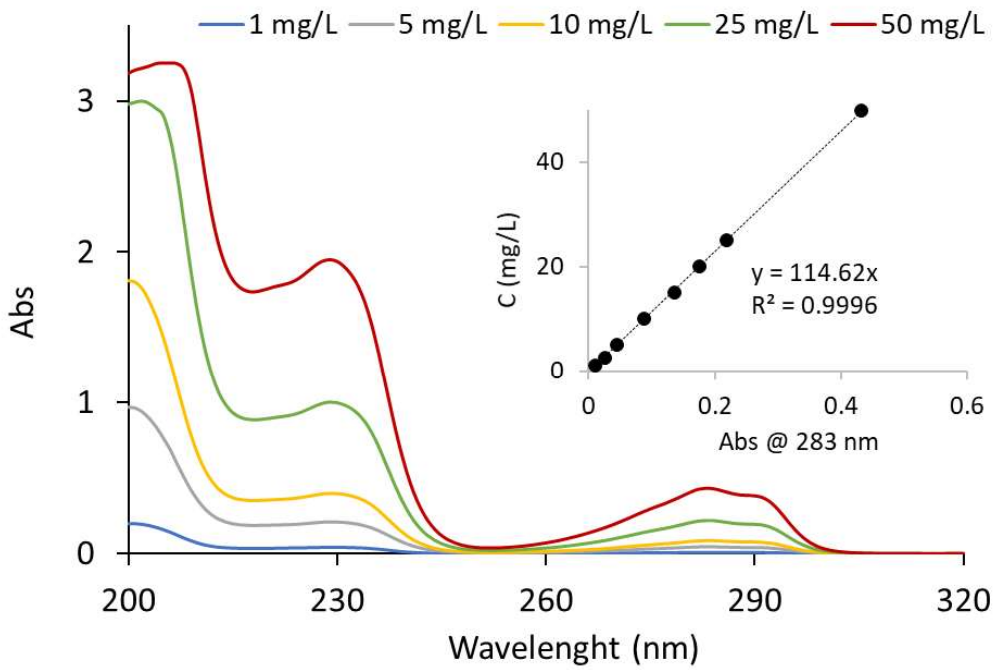

637

638 ***Figure 2.*** *UV spectra of aqueous solutions at different concentrations of 2,4-D. Inset: calibration line*

639 *of absorbance vs 2,4-D concentration*

640

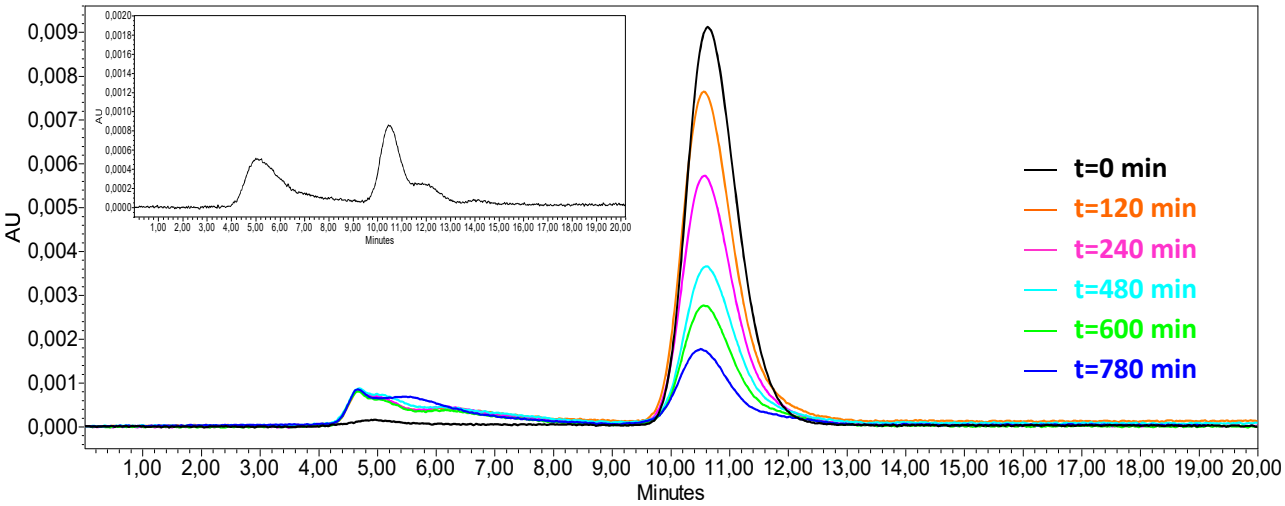

641 ***Figure 3.*** *Example of HPLC chromatograms recorded at 283 nm for samples withdrawn during*

642 *degradation test at 2.5 V. Inset shows HPLC chromatogram for a sample with high conversion of*

643 *2,4-D.*

644

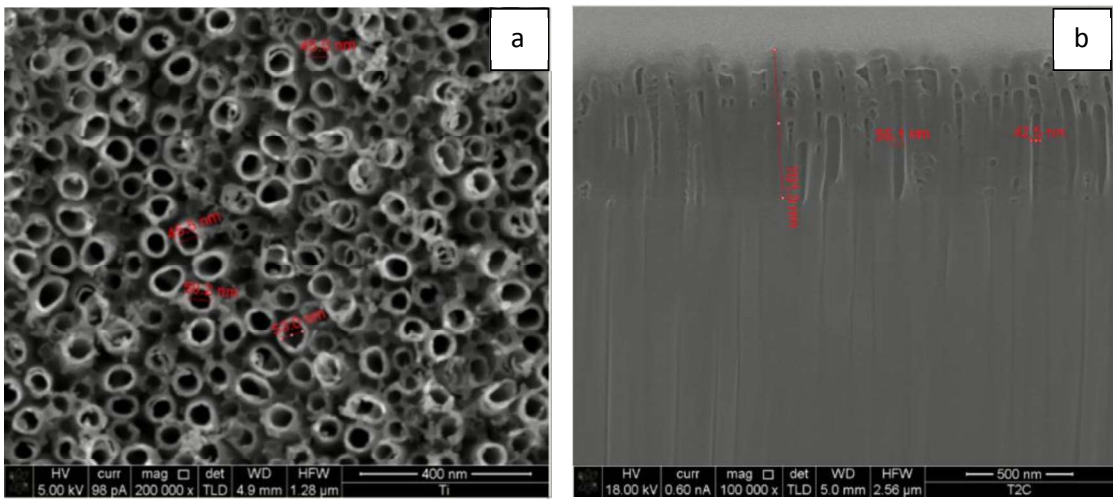

645 ***Figure 4.*** *SEM images of surface (a) and of FIB cross section (b) of TiO_2 nanotubes synthesized in*

646 *glycerol solution.*

647

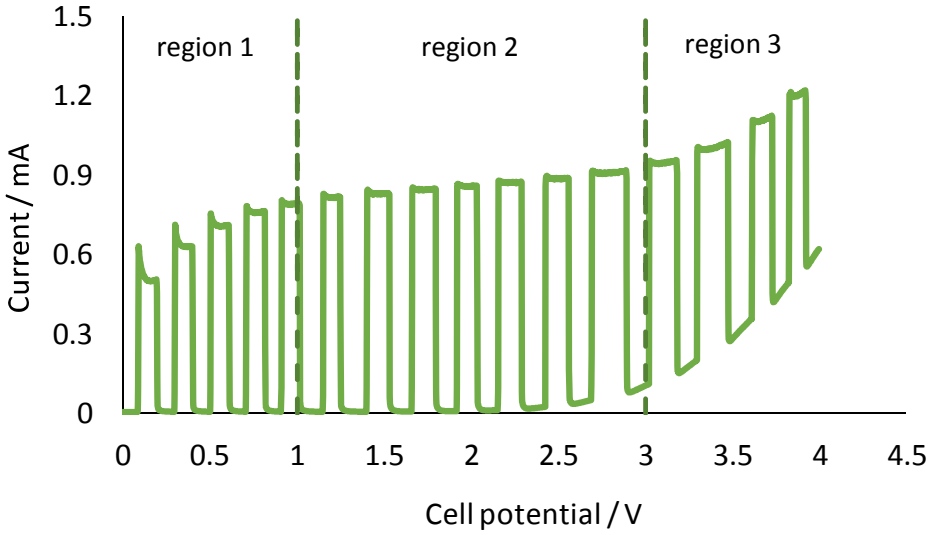

648

649 ***Figure 5.*** *Polarization curve recorded in 50 mg dm^{-3} of 2,4-D (0.1 M $NaClO_4$ supporting electrolyte),*

650 *at a scan rate of 10 mV/s.*

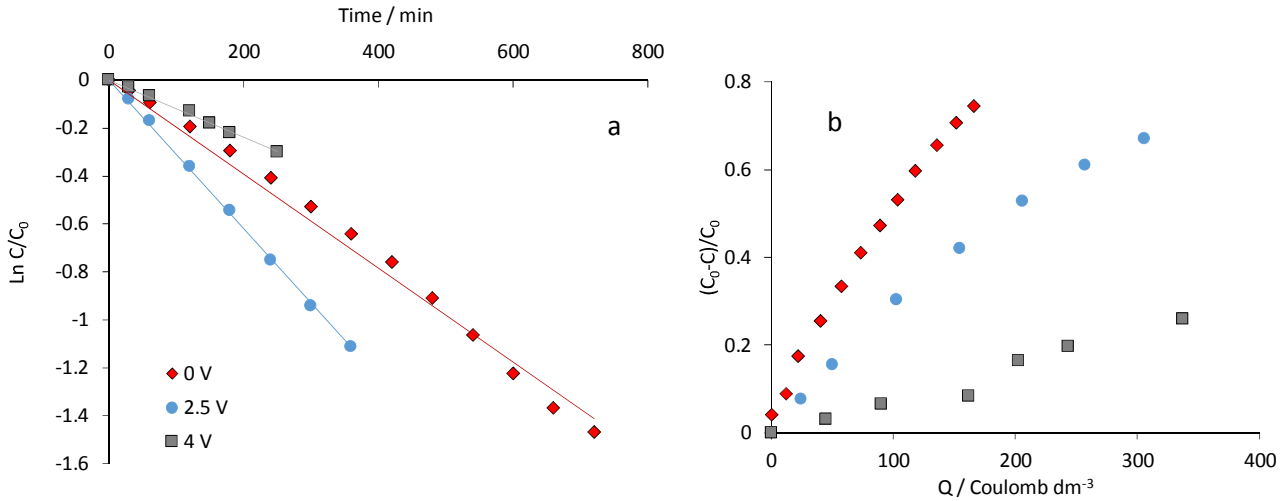

651

652 ***Figure 6.*** *a) Trends of ln C/C_0 vs time during runs performed with 2,4-D solution (C_0 = 50 mg dm^{-3}) at*

653 *different applied potentials. b) fraction of reactant removed as a function of the specific charge*

654 *supplied during the related runs.*

655

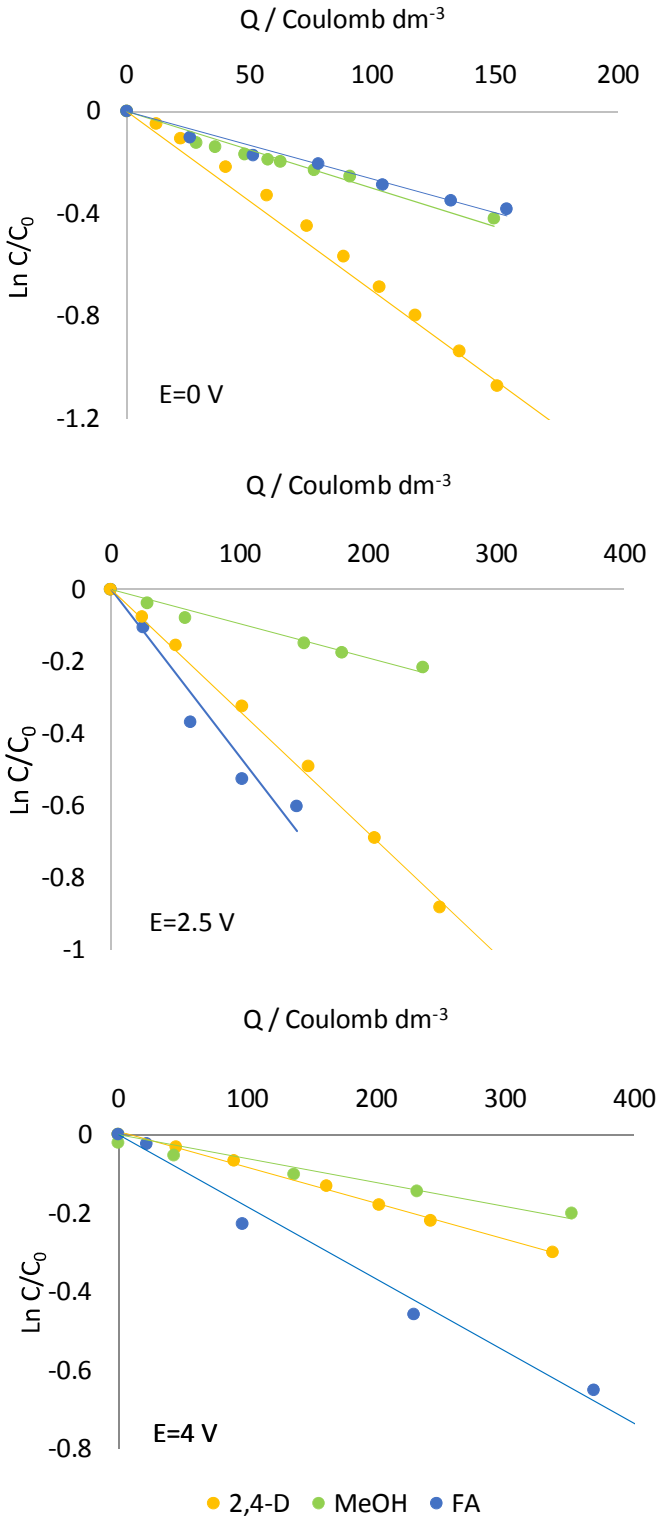

656

657 ***Figure 7.*** *Normalized concentration of 2,4-D vs supplied specific charge, measured during PEC tests*

658 *performed in the three potential regions, in absence or in the presence of scavengers.*

659

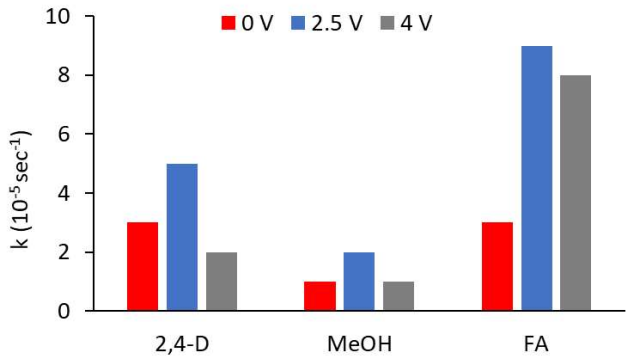

660

661 ***Figure 8.*** *Kinetic constants of the reactant removal process performed in solutions of 50 mg dm^{-3}*

662 *2,4-D, in absence or in the presence of scavengers.*

663

664

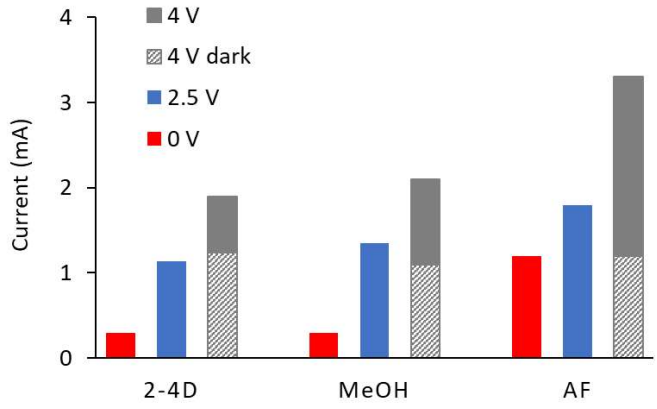

665

666 ***Figure 9.*** *Total currents measured at the electrodes during PEC runs performed in the three potential*

667 *regions, in the presence or in absence of scavenger.*

668

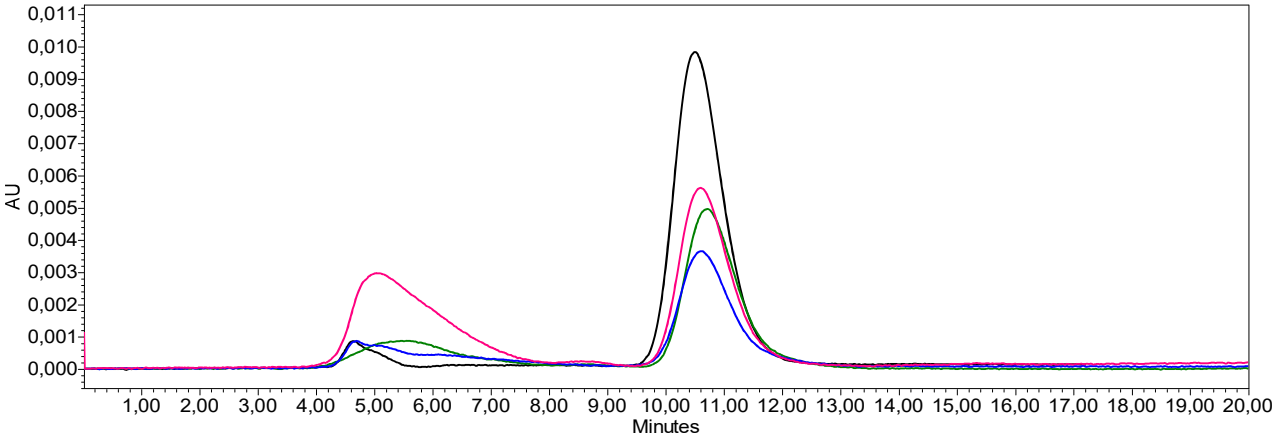

669

670 ***Figure 10.*** *HPLC chromatograms of samples treated under different conditions, being the electric*
671 *charge the same: 4 V (pink line), 2.5 V (green line) and 0 V (blue line). Black line refers to 4 V under*
672 *dark condition.*

673

674

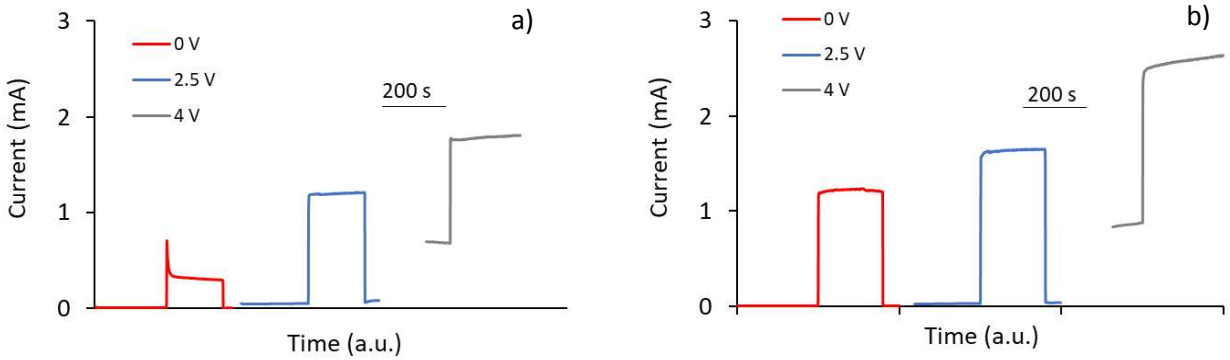

675 ***Figure 11.*** *Potentiostatic tests performed in solutions of 0.2M MeOH (a) or 0.2M FA (b) in 0.1M*
676 *supporting electrolyte. Each scavenger was tested at the three potential ranges (only in the step at*
677 *4 V, the graph does not start from the horizontal axis, due to the contribution of the dark current).*

678

679

680

Captions

Figure 1. *Axonometric sections of the cells used in Ti foil anodization (EC cell -A) and photo-electrochemical tests (PEC cell – B); sketch of the apparatus used for PEC experiments (C).*

Figure 2. *UV spectra of aqueous solutions at different concentration of 2,4-D. Inset: calibration line of absorbance vs 2,4-D concentration*

Figure 3. *Example of HPLC chromatograms recorded at 283 nm for samples withdrawn during degradation test at 2.5 V. Inset shows HPLC chromatogram for a sample with high conversion of 2,4-D.*

Figure 4. *SEM images of surface (a) and of FIB cross section (b) of TiO_2 nanotubes synthesized in glycerol solution.*

Figure 5. *Polarization curve recorded in 50 mg dm^{-3} of 2,4-D (0.1 M $NaClO_4$ supporting electrolyte), at a scan rate of 10 mV/s.*

Figure 6. *a) Trends of ln C/C_0 vs time during runs performed with 2,4-D solution (C_0 = 50 mg dm^{-3}) at different applied potentials. b) fraction of reactant removed as a function of the specific charge supplied during the related runs.*

Figure 7. *Normalized concentration of 2,4-D vs supplied specific charge, measured during PEC tests performed in the three potential regions, in absence or in the presence of scavengers.*

Figure 8. *Kinetic constants of the reactant removal process performed in solutions of 50 mg dm^{-3} 2,4-D, in absence or in the presence of scavengers.*

Figure 9. *Total currents measured at the electrodes during PEC runs performed in the three potential regions, in the presence or in absence of scavenger.*

Figure 10. *HPLC chromatograms of samples treated under different conditions, being the electric charge the same: 4 V (pink line), 2.5 V (green line) and 0 V (blue line). Black line refers to 4 V under dark condition.*

Figure 11. *Potentiostatic tests performed in solutions of 0.2M MeOH (a) or 0.2M FA (b) in 0.1M supporting electrolyte. Each scavenger was tested at the three potential ranges (only in the step at 4 V, the graph does not start from the horizontal axis, due to the contribution of the dark current).*

Captions

Figure 1. *Axonometric sections of the cells used in Ti foil anodization (EC cell -A) and photo-electrochemical tests (PEC cell – B); sketch of the apparatus used for PEC experiments (C).*

Figure 2. *UV spectra of aqueous solutions at different concentrations of 2,4-D. Inset: calibration line of absorbance vs 2,4-D concentration*

Figure 3. *Example of HPLC chromatograms recorded at 283 nm for samples withdrawn during degradation test at 2.5 V. Inset shows HPLC chromatogram for a sample with high conversion of 2,4-D.*

Figure 4. *SEM images of surface (a) and of FIB cross section (b) of TiO_2 nanotubes synthesized in glycerol solution.*

Figure 5. *Polarization curve recorded in 50 mg dm^{-3} of 2,4-D (0.1 M $NaClO_4$ supporting electrolyte), at a scan rate of 10 mV/s.*

Figure 6. *a) Trends of ln C/C_0 vs time during runs performed with 2,4-D solution (C_0 = 50 mg dm^{-3}) at different applied potentials. b) fraction of reactant removed as a function of the specific charge supplied during the related runs.*

Figure 7. *Normalized concentration of 2,4-D vs supplied specific charge, measured during PEC tests performed in the three potential regions, in absence or in the presence of scavengers.*

Figure 8. *Kinetic constants of the reactant removal process performed in solutions of 50 mg dm^{-3} 2,4-D, in absence or in the presence of scavengers.*

Figure 9. *Total currents measured at the electrodes during PEC runs performed in the three potential regions, in the presence or in absence of scavenger.*

Figure 10. *HPLC chromatograms of samples treated under different conditions, being the electric charge the same: 4 V (pink line), 2.5 V (green line) and 0 V (blue line). Black line refers to 4 V under dark condition.*

Figure 11. *Potentiostatic tests performed in solutions of 0.2M MeOH (a) or 0.2M FA (b) in 0.1M supporting electrolyte. Each scavenger was tested at the three potential ranges (only in the step at 4 V, the graph does not start from the horizontal axis, due to the contribution of the dark current).*